Petroleum Science 23 (2026) 2713–2722

Contents lists available at ScienceDirect

Petroleum Science

journal homepage: www.keaipublishing.com/en/journals/petroleum-science

Original Paper

Insights into the charging behavior of tight oil under nanoscale confinement effects

Chuan-Yi Tang [a,b,c], Leng Tian [a,c,*], Song Zhang [d,e,f], Man-Tian Li [d,e,f], Zhen-Tao Yu [d,e,f], You-Guo Yan [g,**]

[a] College of Petroleum Engineering, China University of Petroleum (Beijing), Beijing, 102249, China
[b] Baikouquan Oil Production Plant, Xinjiang Oilfield Company, PetroChina, Karamay, 834000, Xinjiang, China
[c] Research Center for Natural Gas Geology and Engineering, China University of Petroleum (Beijing), Beijing 102249, China
[d] State Key Laboratory of Enhanced Oil & Gas Recovery, Beijing 100083, China
[e] Research Institute of Petroleum Exploration & Development (RIPED), PetroChina, Beijing 100083, China
[f] Key Laboratory of Oilfield Chemistry (KLOC), CNPC, Beijing 100083, China
[g] School of Materials Science and Engineering, China University of Petroleum (East China), Qingdao, 266000, Shandong, China

ARTICLE INFO

Article history:
Received 3 August 2025
Received in revised form
4 November 2025
Accepted 26 December 2025
Available online 31 December 2025

Edited by Meng-Jiao Zhou

Keywords:
Tight oil
Charging behavior
Size effects
The capillary force

ABSTRACT

As conventional oil dwindles, tight oil gains importance for its vast potential. The physical property limit refers to the minimum pore size at which reservoir fluid can be charged under a defined accumulation overpressure, and it is crucial for the accurate assessment of tight oil reservoirs. Micro- and nano-scale pores are the primary storage spaces in tight formations, and the size effect, arising from strong fluid-solid interactions, plays a significant role in influencing the charging behavior of tight oil. However, understanding of tight oil charging in confined space is still limited. In this work, a typical tight oil from the Fengcheng Formation in the Junggar Basin was chosen as the researched objective. Molecular dynamics simulations were employed to investigate the charging process of tight oil into nanoslits pre-occupied by formation water. The critical pressures for tight oil injection into nanoslits with varying sizes were calculated to determine the physical property limit of tight oil charging. Under critical charging conditions, the capillary force acts as the dominant resistance and approximated the threshold charging pressure. The simulated threshold charging pressure was significantly higher than the capillary force predicted by the classic Young-Laplace equation without considering size effects. This result suggests that conventional fluid mechanics theories in confined space overestimate the physical property limit, leading to an inflated assessment of tight oil accumulation. Simulation results show that, as the nanoslit size decreases, interfacial tension and contact angle increase, while water film thickness decreases. By accounting for these size effects, the modified capillary force closely matched the simulated threshold charging pressure. Using the modified capillary force, the physical property limit of tight oil in the Fengcheng Formation, under an accumulation overpressure of 15 MPa, was examined to be 7.2 nm. Furthermore, the effect of mineral types on threshold charging pressure was investigated and give order of illite > calcite > orthoclase > quartz. Additionally, a comparison between the calculated charging pressures with experimentally measured values was conducted, and their strong consistency confirms the validity of the revised Young-Laplace model. This study enhances our understanding of the tight oil charging mechanisms, highlights the importance of size effects, and provides significant insights for the accumulation assessment of tight oil reservoirs.

* Corresponding author.
** Corresponding author.
E-mail addresses: tianleng2008@126.com (L. Tian), yyg@upc.edu.cn (Y.-G. Yan).
Peer review under the responsibility of China University of Petroleum (Beijing).

https://doi.org/10.1016/j.petsci.2025.12.039

1. Introduction

As oil consumption continues to rise and conventional oil resources worldwide become increasingly depleted, petroleum resources in unconventional tight oil reservoirs have garnered significant attention due to its huge development potential (Zaghdoudi et al., 2023). Tight oil is mainly found in low-permeability formations with micro- and nano-scale reservoir space and has become a key part of unconventional hydrocarbon resources (Zeng et al., 2023). Due to the exceedingly small pore throats and complex mineral composition, fluid transport in tight reservoirs differs greatly from that in conventional resources. A critical process in these systems is the charging behavior of tight oil, which involves its migration and accumulation within confined nanoscale spaces. This behavior has a direct impact on tight oil distribution, mobility, and overall recoverability (Zhang et al., 2023a).

In tight reservoirs, oil is frequently driven into reservoir spaces by overpressure caused by geological evolution or stress changes (Xu et al., 2023). The competition between charging resistance and external driving forces plays a critical role in governing the extent and efficiency of tight oil charging (Hu et al., 2023a). The physical property limit, which is the minimum pore size that the tight oil could charge under specific geological conditions, is the key to evaluate the reservoir accumulation (Zhang et al., 2023b). Through detailed characterization of the pore size distribution in the formation matrix, the physical property limit could serve as an efficient method to estimate the volume of reservoir space that can be effectively charged by tight oil, enabling a more precise and reliable evaluation of the accumulation potential in tight oil reservoirs (Ji et al., 2023; Zhong et al., 2023).

In recent years, increasing attention has been directed towards understanding how nanoscale confinement influences the thermophysical properties and dynamic behavior of fluids (Pan et al., 2024). Numerous experimental and simulation studies have demonstrated that size effects can lead to notable deviations in phase behavior, wettability, capillarity, and flow dynamics, all of which exerts a significant influence on hydrocarbon transport (Sun et al., 2018; Zhong et al., 2023). For example, Wei et al. (2022) investigated the transport behavior of graphite nanoparticles in aqueous nanochannels and found that as pore size decreases, interfacial tension increases sharply. Similarly, Alipour and Sakhaee-Pour (2023) observed that the contact angle increases with decreasing pore size, while Chen et al. (2024) confirmed that the effective nanopore size is highly controlled by the adsorbed water film. However, previous research has predominantly focused on phase equilibrium and static adsorption phenomena, the dynamic process of oil charging into nanoslits under overpressure conditions remains relatively underexplored, and the nanoconfinement effect to charging physical limit is unclear. Furthermore, a method to evaluate the threshold charging pressure is urgently needed.

Currently, the rapidly developing molecular dynamics (MD) simulation method has been successfully applied to analyze the microstructure and dynamic evolution of complex systems, enabling the quantitative analysis of molecular interactions (Zhou et al., 2023b). In the field of petroleum exploration and development, MD methods have been widely utilized to study the occurrence characteristics and seepage mechanisms of tight oil (Hu et al., 2023b). However, research specifically focusing on the tight oil charging remains limited. Zhang and Guo (2021) explored the charging process of tight oil in nanopores through molecular dynamics simulations and confirmed that the charging behavior is primarily controlled by the thickness of the adsorbed water film, which varies with different mineral types. As the hydrophilicity of the mineral surface increases, the water film thickness also increases, requiring higher pressure for tight oil charging. They further investigated the effect of associated gases on tight oil charging behavior (Zhang et al., 2023c). Compared to methane, ethane and propane effectively reduce the interfacial tension between oil and water, thereby reducing charging resistance. Despite these advancements, a comprehensive understanding of how fluid properties (interfacial tension, contact angle and water film thickness) in confined space with size effect influence tight oil charging is still lacking, which limits the accumulation evaluation of tight oil reservoirs.

Addressing the issues mentioned, in this work, the MD method was employed to investigate the charging behavior of tight oil into nanoslit pre-occupied by formation water. The threshold charging pressure was calculated by applying spring tension to mimic the tight oil charging. Considering size effect, the interfacial tension, contact angle and effective nanoslit size were calculated to refine the capillary force formula. Using the modified capillary force formula, the physical property limit of tight oil in the Fengcheng Formation was confirmed by combining with the formation overpressure. Our work provided a deep understanding of tight oil charging, and a method was proposed considering the nanoconfinement effect to calculated the threshold charging pressure, which is helpful for reservoir accumulation.

2. Simulation model and methods

2.1. Construction of model

Tight oil model: Tight oil in the Fengcheng Formation of the Junggar Basin is typically found at a depth of 3800 m (Zheng et al., 2020). At this depth, it corresponds to a significant stage of oil generation, with the associated oil primarily consisting of kerogen oil, with R_o approximately 1.0%. By collecting typical samples of the target block, the tight oil composition was determined through experimental characterization with weight ratio of: *n*-dodecane:*n*-heptadecane:*n*-docosane:benzene:phenanthrene:
thioether:asphalt = 15:30:30:7.5:7.5:7:3, and the total density is about 0.84 g/cm^3. Detailed information on the number and molar proportion of tight oil inside nanoslits of different sizes can be found in the Supporting Information, as illustrated in Table S1 and Fig. S1.

Simulation model: Based on the definition of a pore throat as the narrow channel interconnecting pores in rock or soil (Li et al., 2017), a simplified pore throat structure can be constructed using rock lamellae to simulate the reduction of pore size from pore space to narrow pore throats, facilitating the simulation of tight oil charging. Based on X-ray diffraction and nuclear magnetic resonance mineralogical analysis, the tight reservoir in the Fengcheng Formation is composed of various proportions of inorganic minerals, with quartz as the main component (Zheng et al., 2020). Therefore, quartz is selected as the researched mineral and is used to construct nanoslits with width of 6–20 nm. To realistically characterize the hydrophilicity of quartz mineral surfaces, the surfaces of quartz pore throats were hydroxylated and the nanoslit is pre-filled with formation water. A tight oil chamber was placed on the left side to act as oil source, and a rigid argon plate was placed on the leftmost side to prevent escaping of oil. Vacuum layers of 2 nm and 8 nm were placed on the left and right sides of the model, respectively, to prevent contact between the argon plates due to periodicity. The overall box dimensions are $2.5 \times (8.6–23.6) \times 40$ nm^3 (*XYZ*), as shown in Fig. 1.

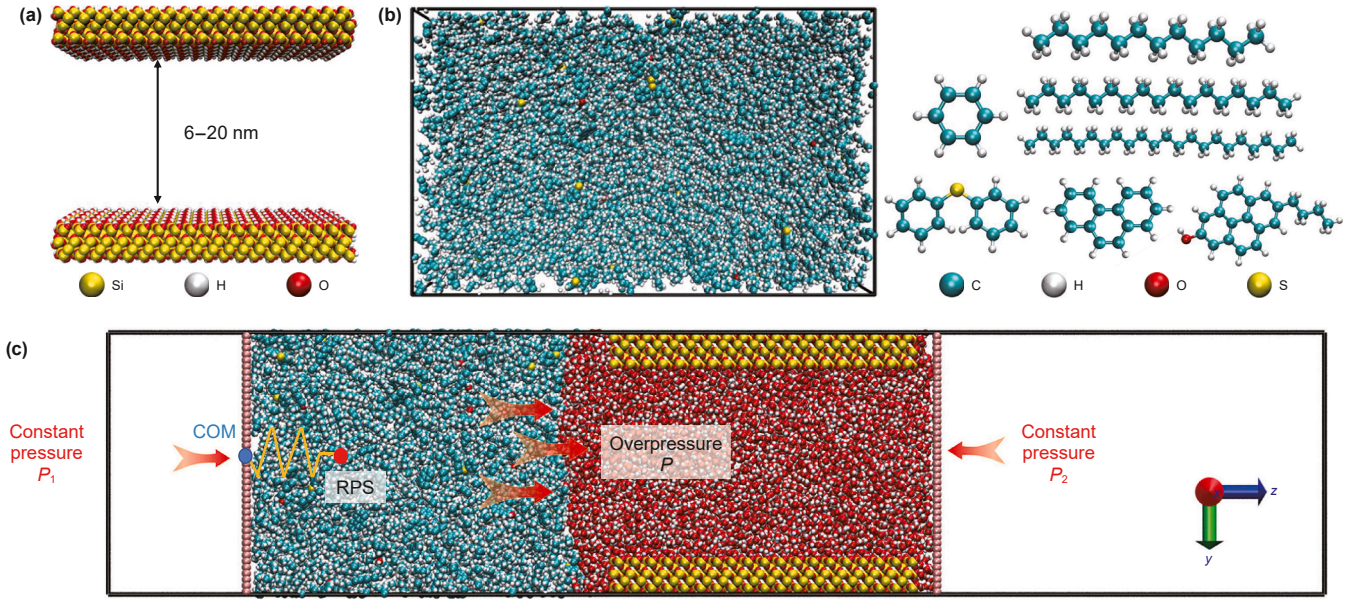

Fig. 1. Molecular structure of (**a**) quartz and (**b**) tight oil, (**c**) initial configuration of tight oil charging in quartz nanochannels, the blue point is the initial center of matter (COM) position of the left argon piston, the red point is the reference point of spring.

2.2. Simulation details

Force fields: Throughout the simulation, the quartz mineral used the Clay-FF force field (Cygan et al., 2004), which has been successfully applied to quartz-fluid systems. The OPLS-AA force field (Jorgensen et al., 1996) was applied for tight oil and the simple point charge (SPC) model (Fuentes-Azcatl et al., 2015) was used to describe water molecules. A detailed discussion about the selection of force field is given in the Supporting Information. All simulations used the 12-6 Lennard-Jones potential and Coulomb potential to describe van der Waals and electrostatic interactions (Wang et al., 2020a), respectively. Long-range electrostatic interactions were calculated using the Particle-Particle Particle-Mesh (PPPM) method (Wang et al., 2020b). All force field parameters are listed in the supplementary material (Table S2).

Equilibrium molecular dynamics (EMD): In this study, all simulation results were obtained using the molecular simulation software of Large-scale Atomic/Molecular Massively Parallel Simulator (LAMMPS) (Thompson et al., 2022) and the simulation snapshots were generated using the visualization software Visual Molecular Dynamics (VMD) 1.9.3 (Humphrey et al., 1996). Following the reservoir conditions of the Fengcheng Formation, a temperature of 423.15 K and a pressure of 31.56 MPa were adopted as the representative conditions in this study. First, the initial configuration was optimized using the steepest descent method. Then, a 6.0 ns equilibrium molecular dynamics (EMD) simulation was performed under the NVT ensemble using a Nosé-Hoover thermostat (Evans and Holian, 1985) until the system reached equilibrium.

Non-equilibrium molecular dynamics (NEMD): To capture the overpressure-driven charging process of tight oil, a time-dependent spring force that gradually increases with time was introduced to simulate its charging behavior within the nanoslit, as displayed in Fig. 1(c). The spring force is obtained through the following equation (Zhang et al., 2020b):

$$F = K((Z_0 + Vt) - Z_{\mathrm{COM}}) \quad (1)$$

where F is the spring force, K represents the spring constant (0.001 kcal·mol^{-1}·nm^{-2} in this work), Z_0 represents the initial center of matter (COM) position of the left argon piston along the Z-axis direction, V is a constant velocity (0.001 nm ps^{-1}) of the reference point of spring (RPS) along the Z-axis, t is the simulation time, and Z_{COM} is the real-time position of the left argon piston COM along the Z-axis at a constant speed. A detailed description about the spring force to mimic the overpressure charging have been added in the supporting information. The three-dimensional periodic boundary conditions were used to this study with a cut-off radius of 12 Å and a time step of 1 fs. The trajectory was saved every 1000 steps for data analysis.

3. Results and discussion

3.1. Tight oil charging into nanoslit

To explore the relationship between overpressure and the physical property limit of tight oil charging, the variation of spring force with simulation time on the left argon piston was calculated, as shown in Fig. 2(a). The results indicate that as the progresses, the spring force gradually increase and finally keeps at constant value, which means that the spring force and the charging resistance reach equivalent. Therefore, the spring force is almost identical in numerical value to the threshold charging pressure. The threshold charging pressure follows the order of 6 nm > 9 nm > 12 nm > 15 nm > 20 nm. Through detailed comparison, it was found that the threshold charging pressure only changes slightly when the nanoslit size is between 9 nm and 20 nm. However, when the nanoslit size is reduced to 6 nm, the threshold charging pressure increases sharply.

In order to reveal the variation, the virtual point position of the spring, the COM position of piston in case of 6 nm nanoslit, and distance between these two positions which is proportional to spring force, were extracted, as shown in Fig. 2(b). The spring force increases continuously as simulation time increases. The variation of spring force could be divided into three stages. At stage I: with the increasing of spring force, tight oil was pushed forward to the nanoslit entrance and a meniscus formed. The meniscus curvature gradually increases along with increase of spring force. At this stage, the distance between the left piston and the virtual point

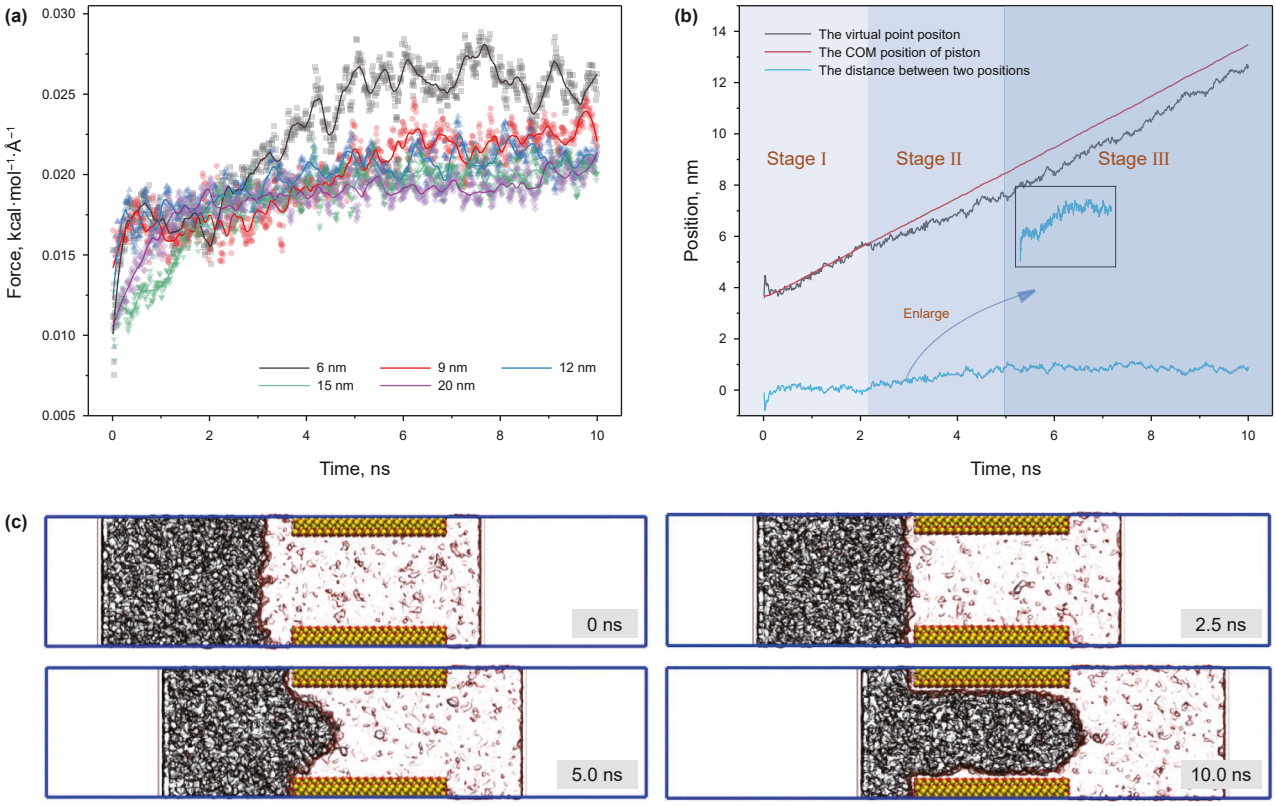

Fig. 2. (**a**) The plots of spring force for different nanoslit sizes, (**b**) the variation trends of the virtual point position and COM position of the piston, (**c**) the snapshots of tight oil charged in 6 nm quartz pore.

has increased, which indicates that the tight oil injection needs to overcome certain resistance. At stage II, once the spring force reaches the threshold charging force (~5 ns in Fig. 2(c)), a maximum meniscus formed and the tight oil could charge into the nanoslit. After that, at stage III, the distance between the left piston and the virtual point remains relatively stable, which suggests a delicate equilibrium between the driving force and resistance force, and the tight oil attains a steady charging state within the nanoslit.

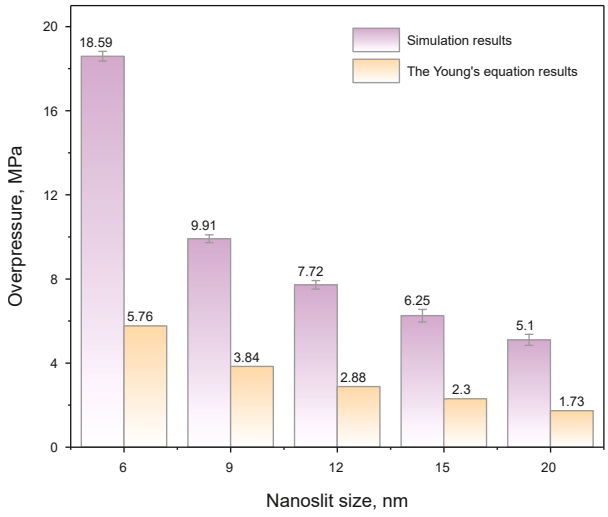

Fig. 3. Calculated threshold charging pressures of tight oil by simulation (purple) and Young's equation (orange) at different nanoslit sizes.

Based on above discussion, the threshold charging resistance is equal to the spring force at stage III, and the average spring force at stage III was statistically calculated. Based on the method of Zhang et al. (2020b), the spring force (kcal·mol^{-1}·Å^{-1}) is converted into the threshold charging pressure (in MPa), yielding the threshold charging pressures corresponding to different nanoslit sizes, as shown in Fig. 3 (purple). A detailed calculation method is included in the supporting information. As shown, with decreasing of nanoslit size, the threshold charging pressure gradually increases and an abrupt increase appears at 6 nm (~18.59 MPa), which largely exceeds the practical overpressure (15 MPa) during tight oil accumulation, meaning the tight oil cannot inject into 6 nm nanoslit in Junggar Basin.

Under critical charging condition, the injection pressure reaches the charge resistance force, the charging could happen. Therefore, the threshold charging pressure can be approximately equal to the charging resistance. As for charging of non-wetting fluid into nanoslit pre-occupied by wetting fluid, the capillary force is the main charging resistance (Hu et al., 2023a). The capillary force can be calculated using the classic Young-Laplace formula, expressed as (Fang et al., 2019):

$$P_s = \frac{2\sigma \cos\theta}{r} \tag{2}$$

where P_s is the capillary pressure, σ is the oil-water interfacial tension, θ is the contact angle, and r is the radius of the nanoslit. The threshold charging pressure calculated by Young-Laplace formula was also depicted in Fig. 3 (orange). It can be seen that the simulation threshold charging pressure is larger than the capillary force calculated from Young-Laplace formula, and the difference become more significant at small-size nanoslit. Based

on aforementioned discussion in section of introduction, the difference mainly comes from the size effect originated from strong liquid-solid interaction inside nanoslit. Therefore, the Young's equation should be corrected with considering size effects, including of interfacial tension (IFT), contact angle and nanoslit size.

3.2. Size effects in tight oil charging

3.2.1. The size effects of the interfacial tension

Base on the Irvine-Kirkwood method, the meniscus is divided into countless thin layers along the direction perpendicular to the nanoslit (y direction) and extracting the pressure components in three directions, the oil/water IFT of various nanoslits were calculated by the following formula (Zhang et al., 2020a), and the detailed calculation details have been added in the supporting informaion.

$$\sigma^2 = \int_0^{\infty} \frac{\mathrm{d}p(r)}{\mathrm{d}r}\mathrm{d}r \int_0^{\infty} r^2 \frac{\mathrm{d}p(r)}{\mathrm{d}r}\mathrm{d}r \tag{3}$$

where σ is the interfacial tension, $p(r)$ is the radial component of the pressure tension, and r is the radius of curvature. The results are shown in Fig. 4. As the nanoslit size decreases, the interfacial tension gradually increases, reaching 19.22 mN/m at 6 nm, showing a linear growth trend. Consequently, a fitting equation, incorporated into Fig. 4, was derived from the interfacial tension trend. This equation enables the prediction of interfacial tension under different slit widths.

Furthermore, the physical nature of the size effect on interfacial tension was discussed. Interfacial tension, which equals the surface free energy, acts as the primary force maintaining the meniscus shape at the front edge of tight oil during the charging process. The surface free energy is regulated by the ordering of water molecules near the quartz walls and increases with the degree of order of the water molecules (De Almeida and Miranda, 2016). Sedghi et al. (2016) found that water molecules exhibit strong directional alignment on the surface of calcite, enhancing the oil-water interactions and thereby increasing the interfacial tension. Herein, the ordering of adsorbed water molecules at different nanoslit size was further calculated, as shown in Fig. 5(a), and a detailed calculation method has been added in the supporting information. As water molecules approach the nanoslit walls, their orientation tends to align parallel to the surfaces, forming an ordered structure with enhanced directional arrangement. This structured ordering becomes more pronounced as the slit width decreases, leading to an increased proportion of adsorbed water near the walls, as shown in Fig. 5(b). Consequently, this phenomenon elevates the gas-water interfacial tension, demonstrating a significant size-dependent effect.

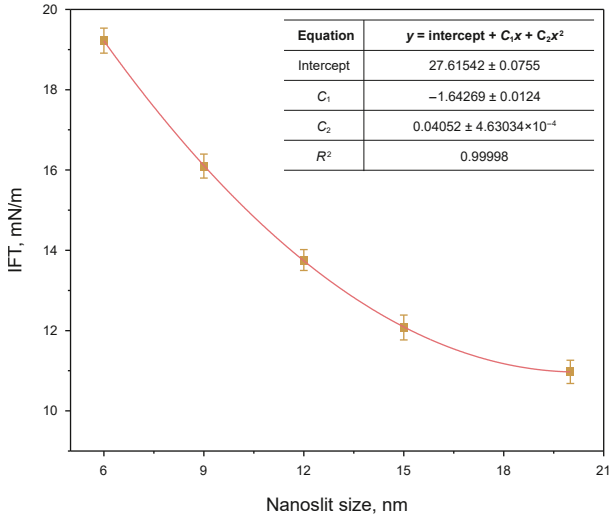

Fig. 4. IFT variation with nanoslit.

3.2.2. The size effects of the water film thickness

Based on the above discussion, the hydrophilic quartz walls exert a strong adsorption effect on water molecules, which in turn induces the directional alignment of water molecules on the quartz surface. When tight oil charges into water-filled quartz slits, the water molecules near the wall cannot be displaced from the slit, as shown in Fig. 2(c). These immobile water molecules gradually form a thin film that coats the quartz surface, which significantly reduces the effective pore size at the nanoscale. To investigate the variation in water film thickness across different pore sizes, the density distribution of water molecules, which are perpendicular to the quartz walls within the slit, was extracted, as illustrated in Fig. 6(a). The smaller the slit width, the greater the density of water molecules on the quartz surface, indicating a higher degree of aggregation. The density distribution reflects the positional distribution of water molecules within the slit following tight oil charging. Therefore, the water film thickness was approximated by calculating the distance from the slit wall to the point where the water molecule density drops to zero in the density distribution. Using this approach, the relationship between water film thickness and slit width was derived, as illustrated in Fig. 6(b). When the slit width exceeds 12 nm, the water film thickness gradually stabilizes. In contrast, when the width is less than 12 nm, the water film thickness decreases significantly as the pore size reduces, exhibiting a distinct size effect.

Furthermore, to more accurately characterize how the effective pore size influences the charging pressure of tight oil, the ratio of water film thickness to nanoslit width was calculated, as illustrated in Fig. 5(b). At a slit width of 6 nm, the water film thickness accounts for the highest proportion of the slit width of 30%, which narrows the effective flow channel for tight oil charging. Consequently, a larger charging force is required to displace the mobile water film adjacent to the quartz surface from the slit. To further clarify the size effect on the water film, the variation of water film thickness with slit width was fitted, as illustrated in Fig. 6(b). The fitted equation can be used to predict variations in water film thickness across different slit widths.

3.2.3. The size effects of the contact angle

As to contact angle of the charging oil within the nanoslit, the stable charging state was selected as the calculation basis. After determining the position coordinates of the tight oil, a clear oil-water interface boundary was obtained. Subsequently, MATLAB software was used to compute the contact angle, with the fitting results and corresponding equation presented in Fig. 7, and the detailed calculation details have been added in the supporting informaion.

As shown, all contact angles of the injected oil in the hydrophilic nanoslit exceed 90°, indicating that the injected oil acts as the non-wetting phase. Consequently, the capillary force is negative, necessitating a certain driving pressure to achieve oil charging. As the nanoslit size decreases, the contact angle approaches 180°, and the meniscus gradually aligns perpendicularly to the quartz surface. The underlying mechanism for this contact angle variation with nanoslit size can be understood as follows: when water molecules interact with the quartz wall, the liquid exhibits strong wetting properties on the solid surface, facilitating

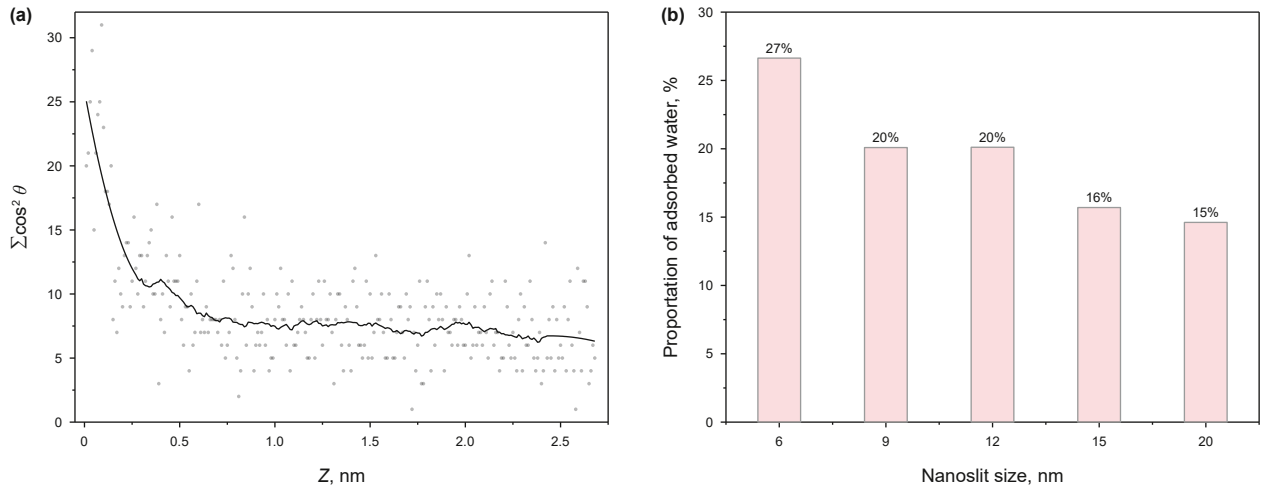

Fig. 5. (**a**) The orderness of water molecules near to the slit surface, (**b**) the proportion of adsorbed water relative to the total water within the nanoslit.

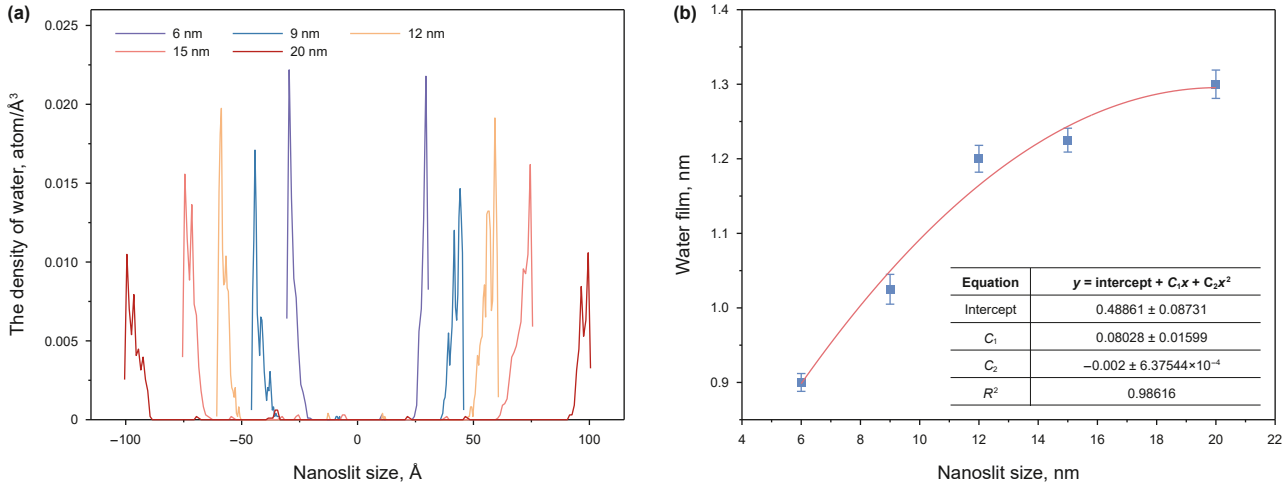

Fig. 6. (**a**) The density of water in nanoslits, (**b**) water film thickness variation with nanoslit size.

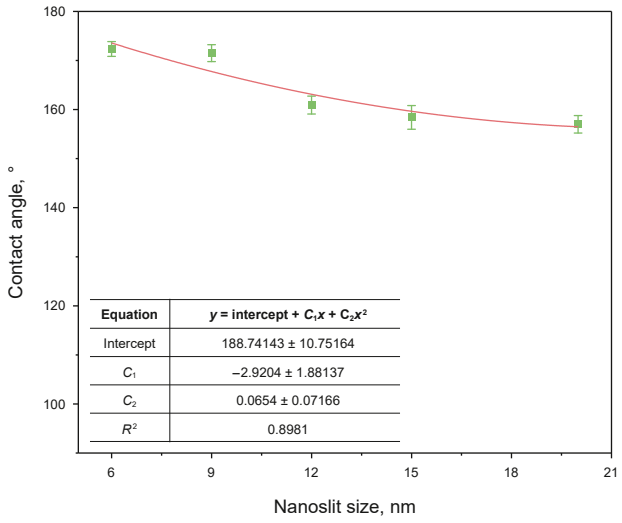

Fig. 7. The contact angle variation with nanoslit size.

the spreading of water along the pore walls. This leads to the formation of a strongly adsorbed water film adjacent to the wall and a weakly adsorbed water film in the region farther from the wall. In larger pores, the weakly adsorbed water film is more easily displaced, leading to a larger meniscus. As shown in Fig. 6(a), the density distribution of water molecules within the nanoslit exhibits multiple adsorption peaks. Water molecules near the wall form hydroxyl bonds with the quartz surface, causing them to aggregate tightly and create a strong adsorption water film (the highest peak). In contrast, the adsorption peak farther from the wall corresponds to water molecules that are drawn by intermolecular forces and loosely adsorbed onto the wall surface. This weakly adsorbed water film exhibits lower stability and can be easily displaced by tight oil, which is why it is termed as weakly adsorbed (other peaks).

Beyond the above discussions, an additional perspective based on disjoining forces has been included in the supporting information to elucidate the size effect on the interface, contact angle, and water film.

3.3. Size effect on charging resistance

Based on the above discussion, it is evident that significant size effect exists in tight oil systems. This effect influences interfacial

tension, contact angle, and the effective size of the nanoslit, thereby increasing the charging resistance of tight oil. The confined space exhibits distinct behaviors compared to the bulk space. When calculating capillary forces, neglecting the size effect in the classical Young-Laplace equation will result in unquantifiable deviations in the evaluation of the physical properties of tight oil systems.

Here, capillary forces were calculated using the classical Young-Laplace equation with and without considering the size effect. These two sets of results were then compared with the simulation results, as illustrated in Fig. 8. It can be observed that as the nanoslit size decreases, the discrepancy between the simulated threshold charging pressure and the capillary force calculated by the uncorrected Young-Laplace equation becomes increasingly pronounced. Specifically, the calculated capillary force underestimates the simulated threshold charging pressure. This finding indicates that the physical property limits derived from traditional fluid mechanics theories are overestimated, which in turn leads to an overvaluation of the accumulation potential of tight oil reservoirs.

By incorporating size effects into interfacial tension, contact angle, and nanoslit size, the capillary forces calculated via the modified Young-Laplace equation align more closely with the simulated threshold charging pressure. This underscores the significance of size effects in evaluating the accumulation potential of tight oil reservoirs. A detailed analysis reveals that for smaller nanoslit sizes, the corrected capillary forces are closer to the simulated threshold charging pressure; in contrast, larger discrepancies emerge for larger nanoslits. This deviation can be attributed to viscous and inertial resistances, which are affected by liquid mass. In small-scale nanoslits, the liquid mass is minimal, rendering the impact of viscous and inertial resistances negligible compared to capillary forces. Conversely, in larger nanoslits, the increased liquid mass enhances the effects of viscous and inertial resistances relative to capillary forces. Consequently, significant discrepancies arise between the simulated threshold charging pressure and the capillary forces calculated via the modified Young-Laplace equation for large nanoslits.

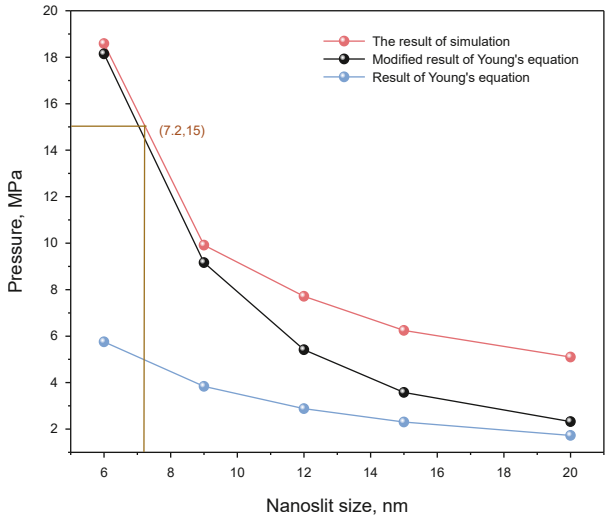

Fig. 8. Simulation result (red), results of Young's equation after correction (black), results of Young's equation before correction (blue), the orange point represents the threshold charging limit of the Fengcheng Formation.

Employed the Fengcheng Formation as example, its typical overpressure is 15 MPa. Based on the simulated threshold charging pressure and capillary force calculated from uncorrected Young-Laplace formula, the physical property limit of the tight oil in Shahezi Formation is about 7.2 nm. However, if the typical Young-Laplace formula is utilized to predict the physical property limit, which is lower than 6 nm. Therefore, the size effect should be considered to evaluate the physical property limit in tight oil charging.

3.4. Effect of mineral types on tight oil charging

Based on the aforementioned discussion, liquid-solid interaction plays a crucial role in determining the distribution and migration of fluids in rock pores, especially for minerals such as clay, feldspar, and quartz (Zhang and Guo, 2021; Zhou et al., 2023a). Their surface properties exert a key influence on fluid wettability, gas-water interfacial tension, and gas migration capacity. In this study, four minerals including of quartz, calcite, orthoclase, and illite were employed to investigate the effect of mineral type on tight oil charging.

The evolution curves of spring force with simulation time in 6 nm slits of quartz, calcite, orthoclase, and illite were calculated. The results indicate that with the progression of charging, the spring forces for all four minerals gradually increase and stabilize at a constant value after a certain period, corresponds to the threshold charging pressure of tight oil, as presented in Fig. 9. Consequently, the thresholds for the four nanoslits follow the order: illite > calcite > orthoclase > quartz, with values of 42.83 MPa, 32.81 MPa, 20.90 MPa, and 18.59 MPa, respectively. Among these, the threshold for the quartz nanoslit is the lowest. Considering the influence of mineral type on the charging process of tight oil, it is inferred that tight oil is likely to preferentially fill quartz nanoslits.

In order to clarify the difference of charging resistance of different mineral types, the changes of effective pore size, interfacial tension and contact angle in Young's equation was investigated. Since the rock walls are hydrophilic walls, it can be seen in Fig. 9(b) that the tight oil charging channel is partially occupied by water molecules. Fig. 10(a) gives the effective nanoslit size for tight oil charging, which equal to the width of the nanoslit minus the thickness of the water film, following the order of quartz ≈ orthoclase > calcite > illite.

As to the interfacial tension, based on above discussion, the strong adsorption of water on mineral surface induce to increased interfacial tension. Therefore, the different adsorption capability of four minerals to water results in different interfacial tension, giving order of illite > calcite > orthoclase > quartz, as presented in Fig. 10(b). In addition, as shown in Fig. 10(c), the contact angles follow the order of illite > calcite > orthoclase > quartz. This indicates that with increasing hydrophilicity of mineral walls, the displacement front of tight oil tends to aggregate into a spherical shape during charging, and the radius of curvature of the oil-water interface decreases. This is consistent with the findings of Teshima et al. (2022). In summary, the charging process of tight oil is sensitive to the mineral type with different hydrophilicity. The water film thickness, contact angle, interfacial tension increases with the enhanced hydrophilicity.

Considering the modified interfacial tension, contact angle, and effective nanoslit size, the capillary force calculated via the revised Young's equation is comparable to the simulated threshold, as presented in Fig. 10(d). Among the four mineral types, the capillary forces follow the order: illite > calcite > orthoclase > quartz. The influence of different mineral types on threshold holds implications for the accumulation of tight oil reservoirs in formations dominated by different minerals.

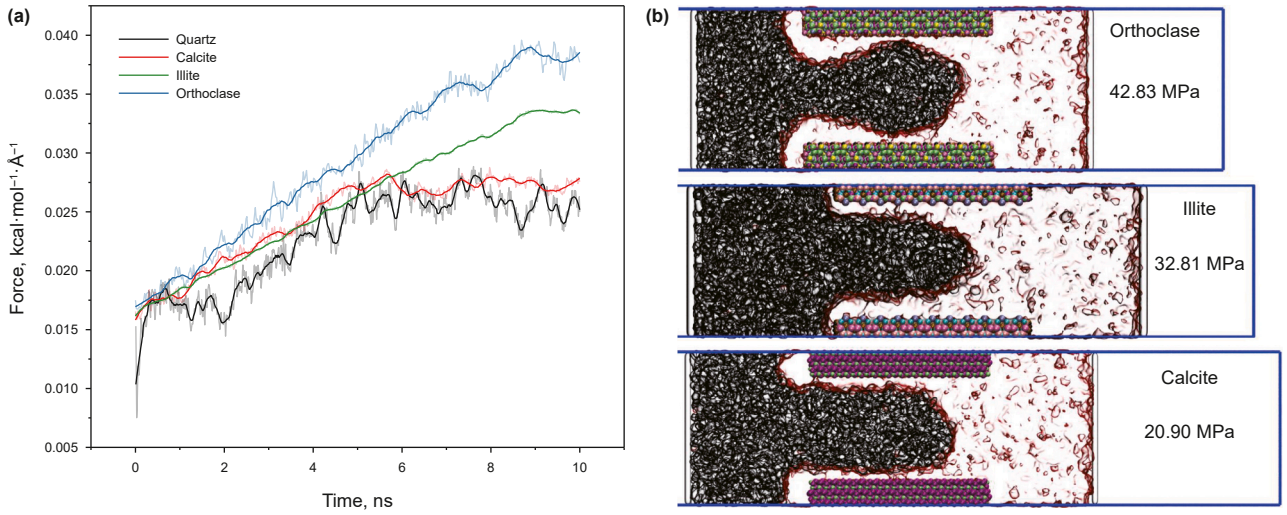

Fig. 9. (**a**) The evolution curve of spring force with simulation time and (**b**) the stable snapshot of tight oil charging and the corresponding threshold of the four mineral types.

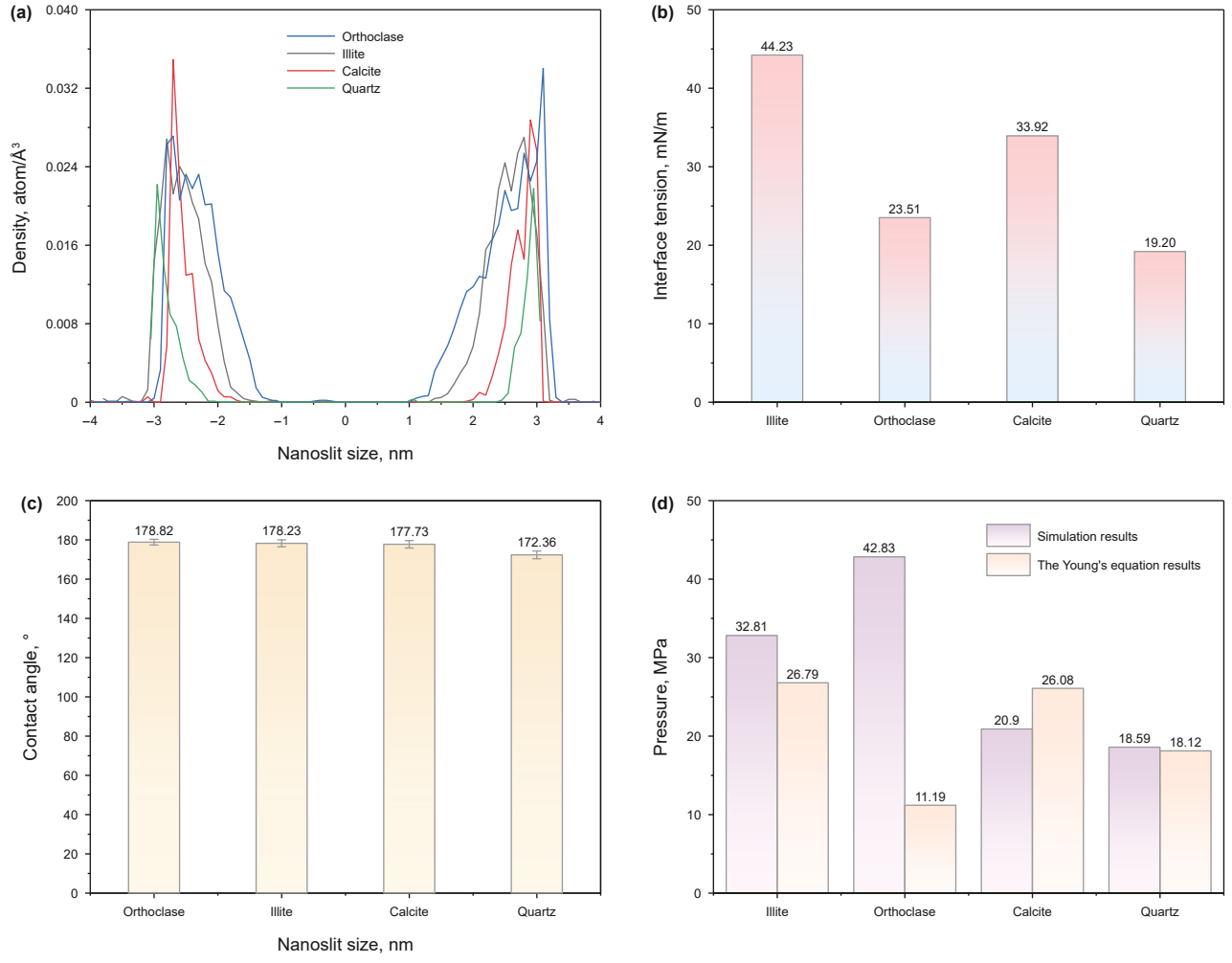

Fig. 10. (**a**) Effective nanoslit size, (**b**) interfacial tension, (**c**) contact angle, and (**d**) comparison of simulation results with modified capillary force for four mineral types.

3.5. Validation of revised Young's formula

To validate the revised Young's formula for predicting physical property limits, we compared the calculated charging pressures with experimentally measured values. Data from high-pressure mercury injection and porosity-permeability measurements in the Changling Fault Depression were analyzed to establish the relationship between the average pore-throat radius and

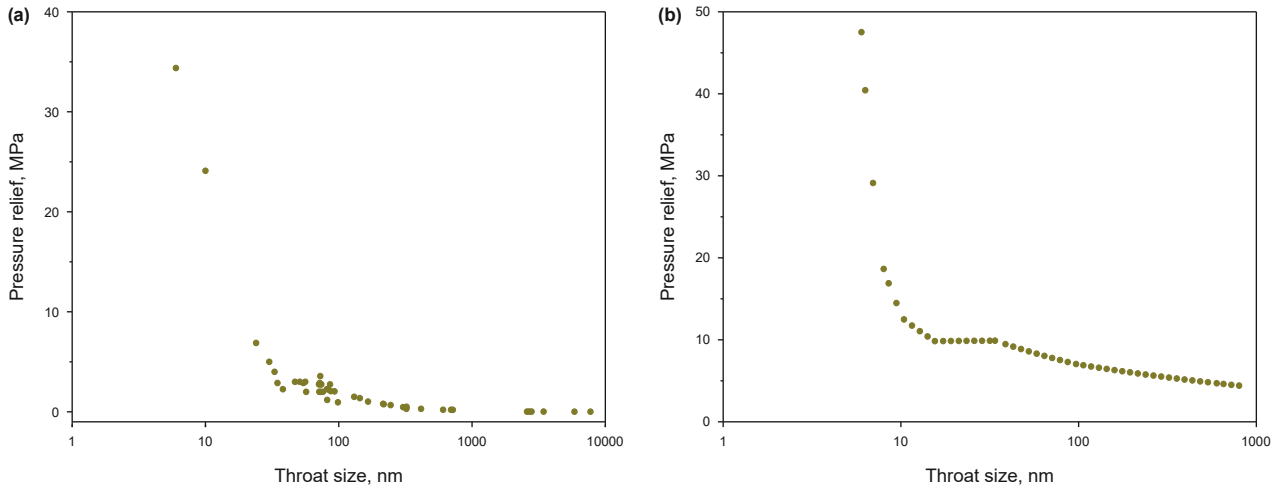

Fig. 11. (**a**) Relationship between pore-throat size and displacement pressure in illite, (**b**) relationship between pore-throat size and displacement pressure in orthoclase.

displacement pressure derived from high-pressure mercury injection. The results reveal a significant negative power-law relationship between the average pore-throat radius and displacement pressure (Fig. 11), indicating that displacement pressure decreases with increasing average pore-throat radius. This trend is consistent with the classical Washburn equation.

The dominant rock type in this case is illite, which exhibits a displacement pressure of 34.9 MPa at a pore-throat radius of 6 nm. Our calculated displacement pressure for this configuration is 32.81 MPa. To further validate our approach, we also incorporated experimental data from the Mahu Sag, where the rock composition is dominated by orthoclase. At a 6 nm pore-throat radius, the measured displacement pressure of orthoclase is 44.95 MPa, which is very close to our calculated value of 43.83 MPa for the orthoclase nanoslit. The strong consistency between experimental measurements and calculated results confirms the validity of the revised Young-Laplace model.

4. Conclusions

In this study, tight oil from the Fengcheng Formation of the Junggar Basin was selected as the research object. Molecular dynamics simulations were employed to investigate the charging behavior of tight oil into water-saturated nanoslits with different sizes. Under critical charging conditions, capillary force dominates the total resistance. Simulation results indicate that the threshold charging pressure obtained from simulations deviates significantly from the capillary force calculated via the classical Young-Laplace equation (without considering size effects). Further analysis reveals that this deviation originates from strong liquid-solid interactions in nanoslits, which induce significant size-dependent effects on interfacial tension, contact angle, and effective nanoslit size. To address this issue, interfacial tension, contact angle, and nanoslit size were revised to incorporate size effects. The capillary force calculated using the corrected Young-Laplace equation shows good agreement with the simulated threshold. Furthermore, the effect of mineral type on threshold charging pressure was also investigated and give order of illite > calcite > orthoclase > quartz, with values of 42.83, 32.81, 20.90, and 18.59 MPa, respectively. In conclusion, the corrected capillary force enables precise assessment of the physical property limits governing tight oil charging. Additionally, the methodology proposed in this study can be extended to investigate the charging mechanisms of other oil/gas accumulations. This work provides insights into the microscopic processes of tight oil charging and offers valuable guidance for evaluating tight oil reservoir accumulation.

CRediT authorship contribution statement

Chuan-Yi Tang: Writing – review & editing, Supervision, Resources. **Leng Tian:** Writing – original draft, Software, Methodology, Formal analysis. **Song Zhang:** Supervision, Investigation. **Man-Tian Li:** Visualization, Methodology, Data curation. **Zhen-Tao Yu:** Software, Project administration. **You-Guo Yan:** Writing – review & editing, Supervision.

Declaration of competing interest

The authors declare that they have no known competing financial interests or personal relationships that could have appeared to influence the work reported in this paper.

Acknowledgments

This work is financially supported by the Natural Science Foundation of Shandong Province (ZR2025MS794), National Science and Technology Major Project (2024ZD1406000, 2024ZD1004300), Key Research and Development Project of Xinjiang Autonomous Region (2024B03002).

Appendix A. Supplementary data

Supplementary data to this article can be found online at https://doi.org/10.1016/j.petsci.2025.12.039.

References

Alipour, M., Sakhaee-Pour, A., 2023. Application of Young-Laplace with size-dependent contact angle and interfacial tension in shale. Geoenergy Sci. Eng. 231, 212447. https://doi.org/10.1016/j.geoen.2023.212447.

Chen, X., Tang, L., Jia, C., Yue, P., Zhang, Z., Liu, W., 2024. Phase behavior of hydrocarbon fluids in shale reservoirs, considering pore geometries, adsorption, and water film. ACS Omega 9 (2), 2104–2112. https://doi.org/10.1021/acsomega.3c03601.

Cygan, R.T., Liang, J.-J., Kalinichev, A.G., 2004. Molecular models of hydroxide, oxyhydroxide, and clay phases and the development of a general force field. J. Phys. Chem. B 108 (4), 1255–1266. https://doi.org/10.1021/jp0363287.

De Almeida, J.M., Miranda, C.R., 2016. Improved oil recovery in nanopores: NanoIOR. Sci. Rep. 6, 28128. https://doi.org/10.1038/srep28128.

Evans, D.J., Holian, B.L., 1985. The Nose–Hoover thermostat. J. Chem. Phys. 83 (8), 4069–4074. https://doi.org/10.1063/1.449071.

Fang, T., Wang, M., Gao, Y., Zhang, Y., Yan, Y., Zhang, J., 2019. Enhanced oil recovery with CO_2/N_2 slug in low permeability reservoir: molecular dynamics simulation. Chem. Eng. Sci. 197, 204–211. https://doi.org/10.1016/j.ces.2018.12.016.

Fuentes-Azcatl, R., Mendoza, N., Alejandre, J., 2015. Improved SPC force field of water based on the dielectric constant: SPC/ε. Phys. A (Amsterdam, Neth.) 420, 116–123. https://doi.org/10.1016/j.physa.2014.10.072.

Hu, S., Tao, S., Wang, M., Pang, Z., Bai, B., Chen, Y., Lu, S., Chen, Y., Yang, Y., Jin, x., Jia, J., Wang, J., Zhang, T., Lin, S., Wu, Y., 2023a. Migration and accumulation mechanisms and main controlling factors of tight oil enrichment in a continental lake basin. Petrol. Explor. Dev. 50, 547–557. https://doi.org/10.1016/S1876-3804(23)60409-4.

Hu, Z., Duan, X., Chang, J., Zhang, X., Zhou, S., Xu, Y., Shen, R., Gao, S., Mu, Y., 2023b. Multiple gas seepage mechanisms and production development research for shale gas reservoirs from experimental techniques and theoretical models. ACS Omega 8 (4), 3571–3585. https://doi.org/10.1021/acsomega.2c05789.

Humphrey, W., Dalke, A., Schulten, K., 1996. VMD: Visual molecular dynamics. J. Mol. Graph. 14 (1), 33–38. https://doi.org/10.1016/0263-7855(96)00018-5.

Ji, L., Xu, F., Lin, M., Jiang, W., Cao, G., Wu, S., Jiang, X., 2023. Rapid evaluation of capillary pressure and relative permeability for oil–water flow in tight sandstone based on a physics-informed neural network. J. Pet. Explor. Prod. Technol. 13 (12), 2499–2517. https://doi.org/10.1007/s13202-023-01682-7.

Jorgensen, W.L., Maxwell, D.S., Tirado-Rives, J., 1996. Development and testing of the OPLS all-atom force field on conformational energetics and properties of organic liquids. J. Am. Chem. Soc. 118 (45). https://doi.org/10.1021/ja9621760 https://doi.org/11225-11236.

Li, Z., Wu, S., Xia, D., Zhang, X., Huang, M., 2017. Diagenetic alterations and reservoir heterogeneity within the depositional facies: A case study from distributary-channel belt sandstone of Upper Triassic Yanchang Formation reservoirs (Ordos Basin, China). Mar. Petrol. Geol. 86, 950–971. https://doi.org/10.1016/j.marpetgeo.2017.07.002.

Pan, Z., Jin, Z., Li, G., Zhang, K., 2024. Assessing subsurface gas storage security for climate change mitigation and energy transition. Geophys. Res. Lett. 51 (14). https://doi.org/10.1029/2024GL109913. e2024GL109913.

Sedghi, M., Piri, M., Goual, L., 2016. Atomistic molecular dynamics simulations of crude oil/brine displacement in calcite mesopores. Langmuir 32 (14), 3375–3384. https://doi.org/10.1021/acs.langmuir.5b04713.

Sun, Z., Shi, J., Wu, K., Xu, B., Zhang, T., Chang, Y., Li, X., 2018. Transport capacity of gas confined in nanoporous ultra-tight gas reservoirs with real gas effect and water storage mechanisms coupling. Int. J. Heat Mass Tran. 126, 1007–1018. https://doi.org/10.1016/j.ijheatmasstransfer.2018.05.078.

Teshima, H., Kusudo, H., Bistafa, C., Yamaguchi, Y., 2022. Quantifying interfacial tensions of surface nanobubbles: How far can Young's equation explain? Nanoscale 14 (6), 2446–2455. https://doi.org/10.1039/D1NR07428H.

Thompson, A.P., Aktulga, H.M., Berger, R., Bolintineanu, D.S., Brown, W.M., Crozier, P.S., in 't Veld, P.J., Kohlmeyer, A., Moore, S.G., Nguyen, T.D., Shan, R., Stevens, M.J., Tranchida, J., Trott, C., Plimpton, S.J., 2022. LAMMPS – A flexible simulation tool for particle-based materials modeling at the atomic, meso, and continuum scales. Comput. Phys. Commun. 271, 108171. https://doi.org/10.1016/j.cpc.2021.108171.

Wang, X., Ramírez-Hinestrosa, S., Dobnikar, J., Frenkel, D., 2020a. The Lennard-Jones potential: When (not) to use it. Phys. Chem. Chem. Phys. 22 (19), 10624–10633. https://doi.org/10.1039/C9CP05445F.

Wang, X., Zhang, Z., Zhang, J., He, J., 2020b. Insight into the pressure-induced displacement mechanism for selecting efficient nanofluids in various capillaries. Environ. Sci. Nano 7 (9), 2785–2794. https://doi.org/10.1039/D0EN00462F.

Wei, Z., Chiricotto, M., Elliott, J.D., Martelli, F., Carbone, P., 2022. Wettability of graphite under 2D confinement. Carbon 198, 132–141. https://doi.org/10.1016/j.carbon.2022.07.019.

Xu, X., Zhang, L., Zeng, L., Li, C., Zhang, L., Zeng, Z., Ren, X., 2023. Effects of overpressure on deep sandstone reservoir quality: A case study of the medium and Lower Jurassic formation in the Shawan Sag, central Junggar Basin, western China. Geoenergy Sci. Eng. 230, 212203. https://doi.org/10.1016/j.geoen.2023.212203.

Zaghdoudi, T., Tissaoui, K., Maaloul, M.H., Bahou, Y., Kammoun, N., 2023. Asymmetric connectedness between oil price, coal and renewable energy consumption in China: Evidence from Fourier NARDL approach. Energy 285, 129416. https://doi.org/10.1016/j.energy.2023.129416.

Zeng, L., Song, Y., Liu, G., Tan, X., Xu, X., Yao, Y., Mao, Z., 2023. Natural fractures in ultra-deep reservoirs of China: A review. J. Struct. Geol. 175, 104954. https://doi.org/10.1016/j.jsg.2023.104954.

Zhang, H., Wang, X., Jia, C., Li, J., Meng, Q.A., Jiang, L., Wang, Y., Bai, X., Zheng, Q., 2023a. Whole petroleum system and hydrocarbon accumulation model in shallow and medium strata in northern Songliao Basin, NE China. Petrol. Explor. Dev. 50 (4), 784–797. https://doi.org/10.1016/S1876-3804(23)60428-8.

Zhang, J., Tao, S., Wu, S., Liu, G., Zhao, W., Li, G., 2023b. Controlling effect of pore-throat structures on tight oil accumulation effectiveness in the upper Cretaceous Qingshankou formation, Songliao Basin. Geoenergy Sci. Eng. 225, 211689. https://doi.org/10.1016/j.geoen.2023.211689.

Zhang, Y., Fang, T., Ding, B., Wang, W., Yan, Y., Li, Z., Guo, W., Zhang, J., 2020a. Migration of oil/methane mixture in shale inorganic nano-pore throat: A molecular dynamics simulation study. J. Pet. Sci. Eng. 187, 106784. https://doi.org/10.1016/j.petrol.2019.106784.

Zhang, Y., Fang, T., Li, R., Yan, Y., Guo, W., Zhang, J., 2020b. Molecular insight into the oil charging mechanism in tight reservoirs. Chem. Eng. Sci. 211, 115297. https://doi.org/10.1016/j.ces.2019.115297.

Zhang, Y., Guo, W., 2021. Molecular insight into the tight oil movability in nano-pore throat systems. Fuel 293, 120428. https://doi.org/10.1016/j.fuel.2021.120428.

Zhang, Y., Li, S., Dou, X., Wang, S., He, Y., Feng, Q., 2023c. Molecular insights into the natural gas regulating tight oil movability. Energy 270, 126895. https://doi.org/10.1016/j.energy.2023.126895.

Zheng, D., Pang, X., Zhou, L., You, X., Liu, X., Guo, F., Li, W., 2020. Critical conditions of tight oil charging and determination of the lower limits of petrophysical properties for effective tight reservoirs: a case study from the Fengcheng Formation in the Fengcheng area, Junggar Basin. J. Pet. Sci. Eng. 190, 107135. https://doi.org/10.1016/j.petrol.2020.107135.

Zhong, G., Li, Y., Zhang, G., Yuan, R., 2023. Determination of lower limit of effective oil filling property of Chang 6_3 member tight sandstone reservoir in central Ordos Basin. Prog. Geophys. 38 (6), 2663–2673. https://doi.org/10.6038/pg2023GG0655 (in Chinese).

Zhou, J., Zhang, C., Ranjith, P.G., 2023a. Behaviours of methane and water in heterogeneous shale nanopores: Effect of water saturation and pore size. Fuel 335, 126675. https://doi.org/10.1016/j.fuel.2022.126675.

Zhou, L., Wang, W., Yan, Y., Zhao, C., Zhong, J., Liu, Y., 2023b. Molecular insight into the occurrence characteristics of deep oil with associated gas methane and the displacement resistance in water flooding in nano-pore throat. Processes 11 (9), 2529. https://doi.org/10.3390/pr11092529.